

# Surface EM waves in 1D Photonic Crystals

J. Martorell

*Dept. d'Estructura i Constituents de la Materia, Facultat Física,  
University of Barcelona, Barcelona 08028, Spain*

D. W. L. Sprung and G. V. Morozov

*Department of Physics and Astronomy, McMaster University  
Hamilton, Ontario L8S 4M1 Canada*

(November 21, 2018)

Accurate analytic approximations are developed for the band gap boundaries and surface waves of a 1D photonic crystal, making use of the semiclassical theory recently developed by the authors. These analytic results provide useful insight on systematics of surface states.

42.70.Qs, 78.67.-n, 03.65.Sq,

## I. INTRODUCTION

Aside from their intrinsic interest, surface electromagnetic waves (SEW) have recently been proposed [1–4] as a way to efficiently inject light into a photonic crystal waveguide, or to extract a focussed beam from a channel. Absent some such mechanism, the insertion and extraction is problematic. In the cited works, the photonic crystal (PC) was a two dimensional array of rods, of infinite length normal to the plane. In this paper we consider SEW on a one-dimensional (1D) PC, for which we recently developed accurate semi-classical approximations.

Surface electromagnetic waves on a 1D PC were observed almost 30 years ago [5] [6]. The basic theory was developed at that time, [7], and can be found in the monograph of Yariv and Yeh [8]. More recently the effect of varying the thickness of the termination layer has been measured experimentally [9,10] and a sensor based on the properties of SEW's has been proposed and demonstrated [11]. In parallel, numerical calculations for SEW's in the bandgaps have been performed, and further aspects of the theory have also been developed [12–15].

Here we study the properties of semi-infinite 1D photonic crystals with termination layers of various thicknesses. The dispersion equation for the SEW's is well known [8]. However, exact results can be obtained only numerically, and to our knowledge, no simple analytic approximations for them have been developed. Accurate approximations not only assist in finding exact solutions, but also clarify the role of the various parameters defining the crystal.

Starting from the dispersion equation, we first derive exact expressions for the critical thicknesses at which SEW solutions appear and disappear. We then introduce approximate analytic forms for the dispersion relation which are valid in specified cases. We also apply the semiclassical method introduced by us in [16] and [17] to SEW's. These semiclassical approximations provide simple and accurate expressions for the bandgap edges. They also suggest a useful empirical parametrization that underlies our analytical approximate forms.

For brevity we will discuss only the case of TE waves.

Because our methods are formally quite different from those recently presented in [15], in Section II we provide a short summary of the transfer matrix approach, in the notation of our previous work [16]. In Section III we re-derive the exact equation for SEW and obtain from it various analytic approximations for a semi-infinite crystal. With these in hand, we discuss systematics of SEW's. In Section IV we apply the semiclassical approximations of [16] to surface waves, and show that the second approximation is very accurate both for the dispersion relation and the bandgap boundaries. This lends support to the parametrization introduced in Section III. In Appendix A we derive some closed analytic expressions for quantities introduced in [16] as infinite series. These allow a better understanding of the role of the various parameters of the PC.

## II. TRANSFER MATRIX APPROACH FOR A PERIODIC CRYSTAL

We study surface waves of the Tamm type, that form at the interface between a uniform medium of low refractive index,  $n_0$ , and a semi-infinite 1-D photonic crystal, capped by a termination layer of the same material but selected width. To clearly separate the periodic bulk from the remaining surface layer, we split the termination layer of index of refraction  $n_1$  and width  $d_c$  into two pieces, of lengths  $d_s + d_t = d_c$ . Then the periodic array that makes the bulk of the crystal consists of “cells” each made of three uniform layers of widths  $d_t$ ,  $d_2$  and  $d_1 - d_t$  whose respective refractive indices are  $n_1$ ,  $n_2$  and  $n_1$ . The cells are reflection symmetric when  $2d_t = d_1$ . A sketch is shown in Fig. 1. The initial cell, extending from  $z = 0$  to  $z = d \equiv d_1 + d_2$  will be given the index 0, the second index 1, and so on, so that the  $p$ -th cell extends from  $pd$  to  $(p+1)d$  and has  $n(z) = n_1$  when  $pd < z < pd + d_t$  or  $pd + d_t + d_2 < z < (p+1)d$  and  $n(z) = n_2$  when  $pd + d_t < z < pd + d_t + d_2$ . As is customary, we will suppose  $n_1 > n_2 > n_0$ . The rest of the cap layer extends from  $z = -d_s$  to 0, and the uniform medium is located to the left of  $z = -d_s$ .

We choose a coordinate system in which the layers have normal vector along OZ. An obliquely incident plane wave defines the OX axis. For monochromatic TE waves the electric field is parallel to the OY axis. As in [16], we write

$$\begin{aligned}\mathbf{E} &= E(z)\hat{\mathbf{e}}_y e^{i(k\beta x - \omega t)} \\ \mathbf{H} &= [H_x(z)\hat{\mathbf{e}}_x + H_z(z)\hat{\mathbf{e}}_z] e^{i(k\beta x - \omega t)},\end{aligned}\quad (1)$$

where  $\omega$  is the angular frequency,  $k = \omega/c$  is the vacuum wavenumber and  $\beta k$  is the (constant)  $x$ -component of the wavevector of modulus  $k(z) = \omega n(z)/c$ . For a TE wave entering the 1-D photonic crystal from a uniform medium, one has

$$\beta = n_0 \sin \theta_0, \quad (2)$$

where  $\theta_0$  is the angle of incidence measured from the normal. Maxwell's equations require that in a periodic medium the  $E(z)$  introduced in eq. 1 satisfies

$$\frac{d^2 E(z)}{dz^2} + k^2(n^2(z) - \beta^2)E(z) = 0, \quad (3)$$

The solutions are well known. In the  $p$ -th cell, the electric field corresponding to TE waves can be written as

$$E(z) = a_p e^{ik_1(z-pd)} + b_p e^{-ik_1(z-pd)} \quad (4)$$

when  $pd < z < pd + d_t$ , and  $k_1 = k\sqrt{n_1^2 - \beta^2} \equiv kn_{1\beta}$ . Similarly

$$E(z) = c_p e^{ik_2(z-pd)} + d_p e^{-ik_2(z-pd)} \quad (5)$$

when  $pd + d_t < z < pd + d_t + d_2$ , and  $k_2 = k\sqrt{n_2^2 - \beta^2} \equiv kn_{2\beta}$ . Also,

$$E(z) = e_p e^{ik_1(z-pd)} + f_p e^{-ik_1(z-pd)} \quad (6)$$

when  $pd + d_t + d_2 < z < (p+1)d$ . Matching these solutions and their derivatives at the two interfaces, one finds the transfer matrix,  $\mathcal{M}$  [**beware**: this matrix is called  $\mathcal{M}^{-1}$  by some authors].

$$\begin{pmatrix} a_{p+1} \\ b_{p+1} \end{pmatrix} = \mathcal{M} \begin{pmatrix} a_p \\ b_p \end{pmatrix} \equiv \begin{pmatrix} A & B \\ B^* & A^* \end{pmatrix} \begin{pmatrix} a_p \\ b_p \end{pmatrix}, \quad (7)$$

with

$$\begin{aligned}A &= e^{ik_1 d_1} \left( \cos k_2 d_2 + \frac{i}{2} \left( \frac{k_1}{k_2} + \frac{k_2}{k_1} \right) \sin k_2 d_2 \right) \\ B &= e^{ik_1(d_1 - 2d_t)} \frac{i}{2} \left( \frac{k_2}{k_1} - \frac{k_1}{k_2} \right) \sin k_2 d_2.\end{aligned}\quad (8)$$

The periodic (Bloch) waves of the infinite crystal are eigensolutions of the transfer matrix

$$\begin{pmatrix} a_{p+1} \\ b_{p+1} \end{pmatrix} = e^{\pm i\phi} \begin{pmatrix} a_p \\ b_p \end{pmatrix} = \mathcal{M} \begin{pmatrix} a_p \\ b_p \end{pmatrix}, \quad (9)$$

and therefore the secular equation is

$$(A - e^{\pm i\phi})(A^* - e^{\pm i\phi}) - |B|^2 = 0, \quad (10)$$

with eigenvalues

$$e^{\pm i\phi} = \text{Re}(A) \pm \sqrt{\text{Re}(A)^2 - 1}, \quad (11)$$

where we have made use of  $\det \mathcal{M} = |A|^2 - |B|^2 = 1$ . The corresponding eigenvectors are, up to a normalization factor

$$\begin{pmatrix} a \\ b \end{pmatrix} = \begin{pmatrix} B \\ e^{\pm i\phi} - A \end{pmatrix}. \quad (12)$$

In allowed bands  $\phi$  is real and the bandgap boundaries are defined by the condition  $\text{Re}A = \pm 1$ . In bandgaps the eigenvalues  $\lambda_{\pm} \equiv e^{\pm i\phi}$  are real since  $|\text{Re}A| > 1$ , and therefore

$$\lambda_{\pm} = \text{Re}(A) \pm \sqrt{\text{Re}(A)^2 - 1}, \quad (13)$$

with  $\lambda_- \lambda_+ = 1$ . We choose the solution that gives a damped wave when  $z \rightarrow +\infty$ . It is  $\lambda_-$  ( $\lambda_+$ ) when  $\text{Re}(A) > 1$  ( $< -1$ .) We write it as simply  $\lambda$  and bear in mind that  $|\lambda| < 1$ .

### III. SURFACE WAVES

These are states which decay in both directions, as one moves away from the surface of the photonic crystal. To the left of  $z = 0$  we have the variable portion of the cap layer, and the uniform external medium. The electric field is written as

$$E(z) = a_s e^{ik_1 z} + b_s e^{-ik_1 z}, \quad (14)$$

when  $-d_s < z < 0$  and

$$E(z) = b_o e^{q_0 z}, \quad (15)$$

with  $q_0 = k\sqrt{\beta^2 - n_0^2}$ , when  $z < -d_s$ . Matching at the interfaces, and choosing the damped wave solution for  $z > 0$ , one finds

$$\frac{q_0}{k_1} = -i \frac{\lambda - A - \tilde{B}}{\lambda - A + \tilde{B}} \quad (16)$$

where for simplicity we absorb a phase into

$$\tilde{B} \equiv e^{-2ik_1 d_s} B. \quad (17)$$

Eq. 16 determines the dispersion relation  $k = k(\beta)$  for the surface waves. It has to be solved numerically, and we will refer to the solutions thereby obtained as "exact".

We begin by examining the structure of eq. 16. From the definitions of  $q_0$  and  $k_1$  given above, we see that the left hand side depends on  $\beta$ , but not on  $k$ . Eq. 10 shows that  $|\lambda - A| = |B| = |\tilde{B}|$ , so that by writing

$$\theta_{\lambda-A} \equiv \arg(\lambda - A) \quad , \quad \theta_{\tilde{B}} = \arg(\tilde{B}) \quad , \quad (18)$$

eq. 16 becomes:

$$\frac{q_0}{k_1} = -i \frac{e^{i\theta_{\lambda-A}} - e^{i\theta_{\tilde{B}}}}{e^{i\theta_{\lambda-A}} + e^{i\theta_{\tilde{B}}}} = \tan\left(\frac{\theta_{\lambda-A} - \theta_{\tilde{B}}}{2}\right) \quad . \quad (19)$$

Next we look at  $\arg(\tilde{B})$ . From eq. 8 we note that

$$\frac{k_2}{k_1} - \frac{k_1}{k_2} = \frac{n_{2\beta}}{n_{1\beta}} - \frac{n_{1\beta}}{n_{2\beta}} < 0 \quad , \quad (20)$$

according to the choice  $n_1 > n_2$  made earlier. Hence,

$$\theta_{\tilde{B}} = \frac{\pi}{2} + kn_{1\beta}(d_1 - 2d_c) + \phi_s \quad (21)$$

with  $\phi_s$  chosen to be 0 or  $-\pi$  depending on the sign of  $\sin k_2 d_2$ . As shown in [15], this sign is characteristic of each bandgap, unless the latter shrinks to zero width in what is called an optical hole [15]. Defining

$$\Theta(\beta) \equiv \tan^{-1}\left(\sqrt{\frac{\beta^2 - n_0^2}{n_1^2 - \beta^2}}\right) \quad , \quad (22)$$

we can rewrite eq. 19 as

$$\theta_{\lambda-A}(k) = 2\Theta(\beta) + kn_{1\beta}(d_1 - 2d_c) + \phi_s + \frac{\pi}{2} + 2\pi\nu \quad (23)$$

with  $\nu = 0, \pm 1, \pm 2, \dots$ . The l.h.s. and the second term on the r.h.s. of this equation depend on  $k$ , while the others do not.

The term  $2\pi\nu$  arises from the inverse of the tangent appearing in eq. 19. When for a given  $\beta$  and  $d_c = d_{c,0}$  the  $\nu = 0$  solution is  $k = k_0$ , one sees easily that  $k = k_0$  is also a solution corresponding to the same  $\beta$  and  $d_c = d_{c,0} + \nu\pi/(n_{1\beta_0}k_0)$ , with  $\nu = \pm 1, \pm 2, \dots$ . This is analogous to the well known property of solutions of the Schrödinger equation for a finite square well potential: increasing the width of the well by a half-wavelength, produces a state of the same energy but one additional node. For simplicity we will focus, from here on, on the case  $\nu = 0$ .

If  $\theta_{\lambda-A}$  was linear or quadratic in  $k$  for fixed  $\beta$ , we could easily solve eq. 23 for  $k(\beta, \dots)$  in terms of the other parameters, and so identify the SEW's. Since that is not the case, one is reduced to numerical or graphical methods of solution. To see how this works, we consider an example in the first bandgap, taken from [16]: a PC with parameters  $n_1 = 2$ ,  $d_1 = 100$  nm,  $n_2 = 1.5$  and  $d_2 = 250$  nm. In Fig. 2 we plot separately the left hand side (continuous line), and the right hand side for several values of  $d_c$  (dashed lines). In the first bandgap,  $\sin k_2 d_2 > 0$  and therefore we have set  $\phi_s = -\pi$ . As  $k$  varies over the bandgap from  $k_L$  to  $k_R$ , the argument  $\theta_{\lambda-A}$  increases from  $-\pi/2$  to  $\pi/2$ . This is a generic feature, as discussed in [18]. The intersection of any dashed line with the continuous line defines a corresponding solution for  $k$ . One

sees that as  $d_c$  decreases the corresponding  $k$  increases, as expected (think of the analogy with the solutions of the Schrödinger equation). The extreme values of  $d_c$  for which a solution exists will therefore be those for which the r.h.s. of eq. 23 takes the values  $\pm\pi/2$ . This gives the values

$$\begin{aligned} d_{c,min} &= \frac{d_1}{2} + \frac{1}{k_R n_{1,\beta}} \left( \Theta(\beta) - \frac{\pi}{2} \right) \\ d_{c,max} &= \frac{d_1}{2} + \frac{1}{k_L n_{1,\beta}} \Theta(\beta) \quad . \end{aligned} \quad (24)$$

In the example shown in the figure, corresponding to  $\beta = 1.2$ , one finds  $d_{c,min} = -27$ . nm and  $d_{c,max} = 86.5$  nm. The negative sign merely indicates that there is a surface wave solution for  $d_c$  ranging from 0 to  $d_{c,max}$ .

To proceed further in the analysis of the SEW solutions requires values for the band edges  $k_L, k_R$ . These will be obtained from our semiclassical approximation [16] in Section IV. Before we delve into that, we first introduce an empirical approximation to  $\theta_{\lambda-A}$  which will be justified by the semiclassical theory. For the first bandgap, we write

$$\theta_{\lambda-A}^{(e)} = \sin^{-1}\left(\frac{k - k_m}{w/2}\right) \quad (25)$$

with  $k_m \equiv (k_R + k_L)/2$  and  $w = k_R - k_L$ . In Fig. 3 we compare the exact and the empirical forms of  $\theta_{\lambda-A}$  for four values of  $\beta$  ranging from  $n_0$  to  $n_2$ . It can be seen that the approximation is quite satisfactory.

Based on the above development, we now derive two analytical approximations for the dispersion relation. The first is valid when the crossing point in Fig. 2 lies in the linear portion of  $\theta_{\lambda-A}$ , while the second is valid near the upper and lower ends of the curve.

### A. Solutions in the middle of the bandgap.

These are of particular interest because the damping is stronger, strongly confining the wave to the surface [9].

Assuming that  $k - k_m \ll w$  we can approximate  $\sin^{-1}(2(k - k_m)/w) \simeq 2(k - k_m)/w$  and eq. 23 then has a solution

$$k \simeq \frac{\Theta(\beta) + k_m/w + \phi_s/2 + \pi(\nu + 1/4)}{1/w + n_{1\beta}(d_c - d_1/2)} \quad . \quad (26)$$

In this way we can easily construct  $k(\beta)$  for a fixed value of  $d_c$ , or conversely, study  $k = k(d_c)$  for fixed  $\beta$ . The role of the bandgap parameters  $k_m$  and  $w$  is also quite easy to analyze. Fig. 4 shows the accuracy of this approximation when  $d_c = 25$  nm. For this example, when  $\beta > 1.4$  the approximation ceases to be valid and one has to resort to other approximations described in the next subsection.

## B. Solutions near the bandgap boundaries.

These approximations will be useful in analyzing the results of experiments like those of Robertson and May [10], where the SEW's appear very close to the boundaries. As seen in Fig. 3, the linear approximation to the arcsine fails near the band boundaries. We discuss solutions near the lower boundary, but similar approximations can be developed for the upper boundary.

When  $k$  is slightly above  $k_L = k_m - w/2$ , it is convenient to introduce  $\zeta > 0$  via

$$k - k_m = -\frac{w}{2}(1 - \zeta). \quad (27)$$

Then

$$\begin{aligned} \sin^{-1}\left(\frac{k - k_m}{w/2}\right) &\simeq -\frac{\pi}{2} + \sqrt{2\zeta} \\ &= -\frac{\pi}{2} + 2\sqrt{\frac{k - k_L}{w}}. \end{aligned} \quad (28)$$

Inserting this into eq. 23 gives

$$2\sqrt{\frac{k - k_L}{w}} + p(k - k_L) = \Lambda \quad (29)$$

with

$$\begin{aligned} p &\equiv n_{1\beta}(2d_c - d_1) \\ \Lambda &\equiv 2\Theta + \phi_s + \pi(2\nu + 1) - k_L p, \end{aligned} \quad (30)$$

and solving for  $k - k_L$

$$k = k_L + \frac{1}{p^2} \left( -\frac{1}{\sqrt{w}} + \sqrt{\frac{1}{w} + p\Lambda} \right)^2. \quad (31)$$

which is the desired solution,  $k = k(\beta)$ , near the lower bandgap boundary. Fig. 5 shows an example of the accuracy of this expression. Furthermore, when  $p\Lambda$  is small compared to  $1/w$  one can expand and find

$$k = k_L + \frac{1}{4}w\Lambda^2, \quad (32)$$

which again manifests the dependence of  $k - k_L$  on  $d_c$  and  $w$ , and allows one to construct  $k = k(\beta)$  very easily. Fig. 5 shows again the validity of this approximation. Note also that the condition  $\Lambda = 0$  determines the location of the zone boundary. Writing it out, one recovers eq. 24, so that eqs. 31 and 32 do not violate this exact relation.

## C. Surface states in the second bandgap

In the examples discussed above we focussed on dispersion relations for SEW in the first bandgap. The specific system considered has no optical holes. However, it does

have an optical hole in the second bandgap, so we examine this situation to clarify what that entails.

In eq. 23, the angle  $\theta_{\lambda-A}$  ranges from  $-\pi/2 + \pi(q - 1)$  to  $\pi/2 + \pi(q - 1)$  in the  $q$ -th bandgap. Following the previous argument we find the critical thicknesses for appearance/disappearance of SEW's to be

$$\begin{aligned} d_{c,min} &= \frac{d_1}{2} + \frac{1}{k_R n_{1,\beta}} \left( \Theta(\beta) + \frac{\phi_s}{2} - \frac{\pi}{2}(q - 1) + \pi\nu \right) \\ d_{c,max} &= \frac{d_1}{2} + \frac{1}{k_L n_{1,\beta}} \left( \Theta(\beta) + \frac{\phi_s}{2} - \frac{\pi}{2}(q - 2) + \pi\nu \right) \end{aligned} \quad (33)$$

In the second bandgap, Fig. 6 shows that an optical hole occurs, where the width of the gap shrinks to zero. (See Section IV and [15] for the exact location.) At the optical hole,  $k_2 d_2 = \pi$ , giving a change of sign of  $\sin k_2 d_2$  at this critical  $\beta = \beta_{oh}$ . Correspondingly, one finds that  $\phi_s = 0$  for  $\beta < \beta_{oh}$  and  $\phi_s = -\pi$  for  $\beta > \beta_{oh}$ . The continuous lines in Fig. 7 show  $d_{c,max}$  and  $d_{c,min}$ , computed from eq. 33 with  $\nu = 0$ . The horizontal dashed lines correspond to various values of  $d_c$ . The plot shows that for  $d_c = 10$  nm, there is a SEW for  $\beta$  less than approximately 1.25, and that the SEW reappears for  $\beta > \beta_{oh}$ . Similarly, for  $d_c = 15$  nm there is a SEW when  $\beta$  is less than approximately 1.325, reappearing for  $\beta > \beta_{oh}$ . For  $d_c = 20$  nm SEW appear for  $\beta < \beta_{oh}$ , and for  $\beta$  greater than approximately 1.4. Finally, for  $d_c = 40$  nm there is a SEW only when  $\beta < \beta_{oh}$ .

Fig. 7 shows surface wave solutions when  $d_c = 0.15d_1$  and  $d_c = 0.40d_1$ , and confirms the above discussion. Note that numerically it is rather difficult to locate the end point of the surface wave solution for  $d_c = 0.15d_1$ , because the solutions run very close to the band boundary. In contrast, eq. 33 and the graph Fig. 7 locate that end point very easily.

## D. Solutions when $\beta > n_2$

In this regime,  $k_2 = k\sqrt{n_2^2 - \beta^2}$  becomes imaginary and we write  $k_2 = iq_2$ . The expressions for  $A$  and  $\tilde{B}$  become

$$\begin{aligned} A &= e^{ik_1 d_1} \left( \cosh q_2 d_2 + \frac{i}{2} \left( \frac{k_1}{q_2} - \frac{q_2}{k_1} \right) \sinh q_2 d_2 \right) \\ \tilde{B} &= -\frac{i}{2} e^{ik_1(d_1 - 2d_c)} \left( \frac{k_1}{q_2} + \frac{q_2}{k_1} \right) \sinh q_2 d_2. \end{aligned} \quad (34)$$

As  $\beta$  increases, the hyperbolic functions soon become very large, giving

$$\begin{aligned} A &\simeq \frac{1}{2} e^{ik_1 d_1 + q_2 d_2} \left( 1 + \frac{i}{2} \left( \frac{k_1}{q_2} - \frac{q_2}{k_1} \right) \right) \\ \tilde{B} &\simeq -\frac{i}{4} e^{ik_1(d_1 - 2d_c) + q_2 d_2} \left( \frac{k_1}{q_2} + \frac{q_2}{k_1} \right), \end{aligned} \quad (35)$$

and therefore:

$$\text{Re}(A) \simeq \frac{1}{2} e^{q_2 d_2} (\cos k_1 d_1 - \Gamma \sin k_1 d_1) \quad (36)$$

with

$$\Gamma \equiv \frac{1}{2} \left( \frac{k_1}{q_2} - \frac{q_2}{k_1} \right) = \frac{1}{2} \frac{n_1^2 + n_2^2 - 2\beta^2}{\sqrt{(n_1^2 - \beta^2)(\beta^2 - n_2^2)}}, \quad (37)$$

which is independent of  $k$ . The stationary points of the quantity in parentheses on the right of eq. 36, are at  $\tan k_1 d_1 = -\Gamma$ . At these points:

$$\text{Re}(A) = (-)^q \frac{1}{2} e^{q_2 d_2} \sqrt{1 + \Gamma^2} \quad (38)$$

Therefore  $\text{Re}(A)$  alternates in sign from one bandgap to the next, and the amplitude of the oscillations is large in most of the range of values of  $q_2$  due to the exponential factor. Writing  $\text{Re}(A) = (-1)^q |\text{Re}(A)|$ , and using eq. 13, we obtain

$$\lambda = (-)^q \left( |\text{Re}(A)| - \sqrt{(\text{Re}(A))^2 - 1} \right) \simeq \frac{(-)^q}{2|\text{Re}(A)|}, \quad (39)$$

which is much smaller than  $|A|$  over most of the bandgap. Therefore

$$\theta_{\lambda-A} \simeq \arg(-A) = -\pi + k_1 d_1 + \tan^{-1} \Gamma, \quad (40)$$

where the last term is independent of  $k$  and therefore  $\theta_{\lambda-A}$  becomes linear in  $k$ . Figure 9 shows the accuracy of eq. 40: beyond  $\beta = 1.6$ , the exact (continuous) and the approximate (dashed) dispersion relations practically coincide. Using this approximation and equating  $\theta_{\lambda-A}$  to  $(q-1)\pi \pm \pi/2$  we get an expression for the bandgap boundaries

$$k_{L,R} = \frac{1}{n_{1\beta} d_1} \left[ q\pi \pm \frac{\pi}{2} - \tan^{-1} \Gamma \right] \quad (41)$$

Figure 10 shows that the band boundaries are quite well reproduced by this approximation. The exception is the lowest boundary when  $\beta < 1.6$ . We can also use the approximation for  $\theta_{\lambda-A}$  to predict the dispersion relation: inserting 40 into eq. 23 and solving for  $k$ , one finds

$$k = \frac{1}{n_{1\beta} d_c} \left[ \Theta + \nu\pi + 3\frac{\pi}{4} + \frac{\phi_s}{2} - \frac{1}{2} \tan^{-1} \Gamma \right]. \quad (42)$$

As figure 10 shows, the exact and the approximate curves for  $k = k(\beta)$  are very close (indistinguishable when  $\beta > 1.6$ ). Again, eq. 42 shows very explicitly the role of  $d_c$  and of the indices of refraction in determining  $k$ .

#### IV. SEMICLASSICAL APPROXIMATIONS

The elements of the transfer matrix can be related to the amplitudes for transmission  $t_B$  and reflection  $r_B$ , for a single cell:

$$\begin{pmatrix} t_B \\ 0 \end{pmatrix} = \begin{pmatrix} A & B \\ B^* & A^* \end{pmatrix} \begin{pmatrix} 1 \\ r_B \end{pmatrix}, \quad (43)$$

that is,  $A = 1/t_B^*$  and  $B = -Ar_B^*$ . The semiclassical expressions for  $r_B$  and  $t_B$  are found in eqs. 35 and 36 of [16] for the first and second approximations discussed in that reference.

#### A. First approximation

In this approximation, and for a single cell, eq. 35 of [16] gives

$$\begin{aligned} r_B^{(1)} &= \frac{-s_q^* \sinh(\gamma_1 d)}{\gamma_1 \cosh(\gamma_1 d) - i\delta_q \sinh(\gamma_1 d)} \\ t_B^{(1)} &= \frac{(-)^q \gamma_1}{\gamma_1 \cosh(\gamma_1 d) - i\delta_q \sinh(\gamma_1 d)}. \end{aligned} \quad (44)$$

Therefore

$$\begin{aligned} A_s^{(1)} &= (-)^q \left( \cosh \gamma_1 d + i \frac{\delta_q}{\gamma_1} \sinh \gamma_1 d \right) \\ B_s^{(1)} &= (-)^q \frac{s_q}{\gamma_1} \sinh \gamma_1 d, \end{aligned} \quad (45)$$

where the subscript  $s$  stands for semiclassical, and the superscript (1) denotes the first approximation introduced in [16]. The explicit expression for  $s_q$  is given below, eq. 46,  $\gamma_1 \equiv \sqrt{|s_q|^2 - \delta_q^2}$  and the detuning from the  $q$ -th Bragg resonance is  $\delta_q = n_{av,\beta}(k - k_B)$ , with  $k_B = q\pi/(n_{av,\beta}d)$ . In addition,  $\gamma_1 d$  is the exponent of the damped wave constant,  $\lambda$ , as we can easily confirm: inserting  $\text{Re}A_s^{(1)}$  into eq. 13 we find  $\lambda_s^{(1)} = (-)^q e^{-\gamma_1 d}$ .

Using expressions from [16], for an asymmetric cell we can write  $s_q$  in compact form

$$s_q = -\frac{i}{d} \ln \frac{n_{1\beta}}{n_{2\beta}} e^{i(\phi_1 + \phi_2)/2} \sin((\phi_1 - \phi_2)/2) \quad (46)$$

$$\begin{aligned} \text{with } \phi_1 &= 2(-k_1 + \delta_q)d_t \\ \phi_2 &= 2(-k_1 d_t - k_2 d_2 + \delta_q(d_t + d_2)). \end{aligned} \quad (47)$$

From eq. 45 we find

$$\lambda_s^{(1)} - A_s^{(1)} = (-)^{(q-1)} \sinh(\gamma_1 d) \left( 1 + i \frac{\delta_q}{\gamma_1} \right), \quad (48)$$

and therefore  $\theta_{\lambda_s^{(1)} - A_s^{(1)}}$

$$\begin{aligned} &\equiv \arg(\lambda_s^{(1)} - A_s^{(1)}) = (q-1)\pi + \tan^{-1} \frac{\delta_q}{\gamma_1} \\ &= (q-1)\pi + \sin^{-1} \frac{\delta_q}{|s_q|} \simeq (q-1)\pi + \sin^{-1} \frac{\delta_q}{S_B}, \end{aligned} \quad (49)$$

where in the last step we have replaced the slowly varying  $|s_q(k)|$  by  $S_B$ , its value at the Bragg resonance  $k = k_B$ . Since by definition,  $\delta_q = (k - k_B)n_{av,\beta}$ , we arrive at

$$\theta_{\lambda_s^{(1)} - A_s^{(1)}} \simeq (q-1)\pi + \sin^{-1} \left( \frac{k - k_B}{w/2} \right), \quad (50)$$

with  $w = 2S_B/n_{av,\beta}$ . This has the same form as the empirical parametrization used above, but provides explicit estimates for the width and position  $k_m = k_B$  of the bandgap.

### B. Second approximation

The second, and more accurate, approximation introduced in [16] leads to similar but more involved expressions for  $A^{(2)}$  and  $B^{(2)}$ . From eq. 36 of that reference, we find

$$\begin{aligned} A_s^{(2)} &= (-)^q \left[ \cosh \gamma_2 d \right. \\ &\quad \left. + i \frac{[(1 + |u|^2)\eta_q - 2\text{Im}(s_q u^*)]}{(1 - |u|^2)\gamma_2} \sinh \gamma_2 d \right] \\ B_s^{(2)} &= (-)^q \frac{s_q - 2i\eta_q u - s_q^* u^2}{(1 - |u|^2)\gamma_2} \sinh \gamma_2 d. \end{aligned} \quad (51)$$

where  $\gamma_2 \equiv \sqrt{|s_q|^2 - \eta_q^2}$  and  $\eta_q = \delta_q - ic_2$ . In the appendix we give new analytic expressions for  $u = v_1(z=0)$  and for  $c_2$ , that sum the series written in [16], eqs. 18 and 19. As in the previous case, one easily finds that  $\lambda_s^{(2)} = (-)^q e^{-\gamma_2 d}$ .

Inserting  $A_s^{(2)}$  and  $B_s^{(2)}$  into eq. 16, and solving, one finds the corresponding predictions for  $k = k(\beta)$ . Before presenting these results, we will show the usefulness of this second approximation in giving accurate values for the bandgap boundaries.

In eqs. (31) and (32) of ref. [16] we showed that the first approximation provides simple estimates for the bandgap boundaries. In the second approximation, the condition  $\gamma_2 = 0$  defines the band boundaries, because it corresponds to infinite decay length of the surface state. Using the explicit form of  $\gamma_2$  from eq. (25) of [16], we can write this condition, for the  $q$ -th bandgap boundaries, as

$$\begin{aligned} -|s_q(k_L)| &= (k_L - k_B)n_{av,\beta} + r_2 \\ |s_q(k_R)| &= (k_R - k_B)n_{av,\beta} + r_2, \end{aligned} \quad (52)$$

where  $r_2 \equiv -ic_2$ . The dependence of  $|s_q|$  on  $k$  is fairly smooth as long as  $k$  remains within a bandgap. To a good approximation one can expand around  $k = k_B$  and write

$$|s_q(k)| = S_B + \xi(k - k_B) - \frac{1}{2}\eta(k - k_B)^2, \quad (53)$$

with

$$S_B \equiv |s_q(k_B)| = \frac{1}{d} \ln \left( \frac{n_{1,\beta}}{n_{2,\beta}} \right) \sin \alpha_B.$$

$$\begin{aligned} \alpha_B &\equiv \pi q \frac{n_{2,\beta} d_2}{n_{av,\beta} d} \\ \rho &\equiv \frac{d_1 d_2}{d} (n_{2,\beta} - n_{1,\beta}) \\ \xi &\equiv \frac{1}{d} \ln \left( \frac{n_{1,\beta}}{n_{2,\beta}} \right) \rho \cos \alpha_B \\ \eta &\equiv \frac{1}{d} \ln \left( \frac{n_{1,\beta}}{n_{2,\beta}} \right) \rho^2 \sin \alpha_B. \end{aligned} \quad (54)$$

Inserting this expansion into each line of 52 leads to the desired analytic expressions

$$\begin{aligned} k_L &= k_B + \frac{1}{\eta} \left[ n_{av,\beta} + \xi \right. \\ &\quad \left. - \sqrt{(n_{av,\beta} + \xi)^2 + 2\eta(S_B + r_2)} \right] \\ k_R &= k_B + \frac{1}{\eta} \left[ -n_{av,\beta} + \xi \right. \\ &\quad \left. + \sqrt{(n_{av,\beta} - \xi)^2 + 2\eta(S_B - r_2)} \right] \end{aligned} \quad (55)$$

with  $r_2$  evaluated at  $k = k_B$ :

$$r_2 = \frac{d_1 - d_2}{4d^2} \left( \ln \left( \frac{n_{1,\beta}}{n_{2,\beta}} \right) \right)^2 \sin(2\alpha_B). \quad (56)$$

In Fig. 6 we compare the exact bandgap boundaries to those of eq. 55 and, as can be seen, the latter works very well except very close to  $\beta = n_2$ , where the semiclassical approximation is expected to fail. For  $\beta$  close to  $n_0$  the values of  $\eta$  are small and one can neglect them in eq. 53. This leads to simpler forms:

$$\begin{aligned} k_L &= k_B - \frac{S_B + r_2}{n_{av,\beta} + \xi} \\ k_R &= k_B + \frac{S_B - r_2}{n_{av,\beta} - \xi}. \end{aligned} \quad (57)$$

Neglecting the contribution from  $r_2$  we recover the expressions of the first approximation ( $\gamma_1 = 0$ ) already discussed in [16].

Direct inspection of the expression for  $\text{Re}(A)$  derived from eq. 8 shows that the points where the bandgaps shrink to zero width correspond to special values of the optical depths of the layers:  $k_1 d_1 = m_1 \pi$ ,  $k_2 d_2 = m_2 \pi$ , with  $m_1, m_2$  integers. These give

$$n_{1,\beta} d_1 m_2 = n_{2,\beta} d_2 m_1, \quad (58)$$

so that:

$$\beta_{oh}^2 = \frac{n_1^2 d_1^2 m_2^2 - n_2^2 d_2^2 m_1^2}{d_1^2 m_2^2 - d_2^2 m_1^2} \quad (59)$$

and  $k_{oh} = m_1 \pi / (d_1 n_{1,\beta_{oh}})$ , in agreement with [15]. The point where the second bandgap shrinks to zero width, in Fig. 6, corresponds to  $m_1 = m_2 = 1$ ,  $q = 2$ . It is easy to

check that with the above semiclassical approximations one finds exactly the same optical hole. Note that at this critical value

$$\alpha_B = \pi q \frac{k_2 d_2}{k_1 d_1 + k_2 d_2} = \pi q \frac{m_2}{m_1 + m_2} = \pi \quad (60)$$

so that  $r_2 = 0$ ,  $S_B = \eta = 0$ , and therefore

$$k_L = k_R = k_B . \quad (61)$$

### C. Results for SEW's

In Fig. 11 we compare the exact and semiclassical results for  $k = k(\beta)$ , choosing three thicknesses for the cap layer:  $d_c = d_t = 25, 50$  and  $75$  nm. The first approximation becomes inaccurate when  $\beta$  exceeds 1.4, but gives accurate results up to that value. The second approximation is so close to the exact values that one can see the difference only for values of  $\beta$  very close to the critical value  $\beta = n_2 = 1.5$ . Beyond that, our semiclassical approximations cannot be applied, since  $k_2$  becomes imaginary. In the second bandgap, the accuracy of the first approximation is significantly worse, whereas the second approximation is as good as for the first bandgap. For brevity, we do not show any figures for  $A$  and  $B$  as functions of  $k$  and  $\beta$ . For most of the values in the first bandgap the agreement is similar to that seen in fig. 11 for the dispersion relations.

## V. SUMMARY AND CONCLUSIONS

By considering the semi-infinite limit of a 1D PC we have derived a dispersion equation for SEW's, valid for termination layers of selected width. Our goal has been to clarify the systematics of the solutions of this equation. To do so we first discussed a graphical solution. This allowed us to derive analytic expressions for the critical thicknesses at which solutions appear at the bandgap boundaries. Further, by introducing a suitable parametrization of  $\theta_{\lambda-A}$ , 25, we have derived simple approximations for solutions either in the middle of the bandgap or near the edges: eqs. 26, 31, and 32. We tested them by an example whose first bandgap has no optical holes. We then extended the analysis of critical thicknesses to the second bandgap, where there *is* an optical hole. The appearance and disappearance of solutions as a function of cap layer thickness is again easily predicted: eq. 33. For completeness we have also examined solutions when  $\beta > n_2$ , and again found very simple approximations eqs. 41 and 42, valid over most of the range  $n_2 < \beta < n_1$ , that allow us to study the systematics in a transparent way.

Finally, in section IV, we applied the semiclassical approximations derived in [16] to SEW's. The second approximation is very accurate in predicting the bandgap

boundaries and the dispersion relation. We took advantage of this to derive accurate and simple approximations for the boundaries: eqs. 56 and 57. The first approximation already supports the validity of the empirical parametrization of  $\theta_{\lambda-A}$ : cf. eqs. 25 and 50.

In conclusion: we have presented a set of analytic results, exact and approximate, that clarify the systematics of solutions for surface EM waves in semi-infinite 1D photonic crystals. In addition, we have found simple analytic expressions for the bandgap boundaries that should be useful for the design of PC configurations. We plan next to extend our results to layered configurations with cylindrical symmetry [20,21]. It would also be interesting to see whether the systematics found here apply to surface states in 2D and/or 3D photonic crystals.

## VI. ACKNOWLEDGEMENTS

We are grateful to NSERC-Canada for Discovery Grant RGPIN-3198 (DWLS), and to DGES-Spain for continued support through grants BFM2001-3710 and FIS2004-03156 (JM).

### APPENDIX A: CLOSED FORMS FOR SERIES USED IN THE SEMICLASSICAL APPROXIMATIONS

#### 1. Analytic expression for $u = v_1(0)$

The function  $v_1(z)$  is defined in eq. 19 of [16] as

$$v_1(z) = -\frac{id}{2\pi} \sum_{m \neq q} \frac{s_m e^{i2\pi(m-q)z/d}}{m - q - \delta_q d/\pi} \quad (A1)$$

with  $s_m$  given in eq. 12 of [16]. In the case of interest here, the refractive index is piece-wise *constant*, so that

$$s_m = \frac{1}{2d} \sum_j \ln \frac{n_e(z_j + 0)}{n_e(z_j - 0)} e^{2i(-\psi(z_j) + kn_{av,\beta} z_j - \pi m z_j/d)} \quad (A2)$$

and  $n_e(z) \equiv \sqrt{n^2(z) - \beta^2}$ . Therefore

$$v_1(z) = -\frac{i}{4\pi} \sum_j e^{2i(-\psi(z_j) + kn_{av,\beta} z_j - \pi q z_j/d)} \ln \frac{n_e(z_j + 0)}{n_e(z_j - 0)} \sum_{m \neq q} \frac{e^{i2\pi(m-q)(z-z_j)/d}}{m - q - \delta_q d/\pi} . \quad (A3)$$

Using eqs. 1.445.7 and 8 of [19], we find

$$v_1(z) = -\frac{i}{4} \sum_j \ln \frac{n_e(z_j + 0)}{n_e(z_j - 0)} e^{2i(-\psi(z_j) + kn_{av,\beta} z_j - \pi q z_j/d)} \cdot \left[ \frac{1}{\delta_q d} - \frac{e^{i[(2(\bar{z}-z_j)/d-1)\delta_q d]}}{\sin \delta_q d} \right] , \quad (A4)$$

with  $\bar{z} = z$  when  $0 < z - z_j < d$  and  $\bar{z} = z + d$  when  $z - z_j < 0$ .

For the asymmetric cell of the photonic crystal of interest and  $z = 0+$ , this gives:

$$u = v_1(0+) = -\frac{i}{4} \ln \frac{n_{2\beta}}{n_{1\beta}} \left[ e^{i\phi_1} \left( \frac{1}{\delta_q d} - \frac{e^{i(1-2d_t/d)\delta_q d}}{\sin(\delta_q d)} \right) - e^{i\phi_2} \left( \frac{1}{\delta_q d} - \frac{e^{i(1-2(d_2+d_t)/d)\delta_q d}}{\sin(\delta_q d)} \right) \right]. \quad (\text{A5})$$

with  $\phi_1$  and  $\phi_2$  given in eq. 47.

## 2. Analytic expression for $c_2$

According to eq. 18 of [16]:

$$c_2 \equiv \frac{id}{2\pi} \sum_{m \neq q} \frac{|s_m|^2}{m - q - \delta_q d/\pi}, \quad (\text{A6})$$

and using eqs. 46 and 47, we have

$$c_2 = \frac{i}{2\pi d} \left( \ln \left( \frac{n_{2,\beta}}{n_{1,\beta}} \right) \right)^2 S_2 \quad \text{with} \\ S_2 \equiv \sum_{m \neq q} \frac{\sin^2(Pm + T)}{m - q - \epsilon}, \quad (\text{A7})$$

where

$$P \equiv \pi \frac{d_2}{d}, \quad T \equiv \frac{kd_1 d_2}{d} (n_{2,\beta} - n_{1,\beta}) \quad (\text{A8})$$

and  $\epsilon = \delta_q d/\pi$ . Using eqs. 1.445.6 to 8 of [19] we arrive at:

$$S_2 = \frac{\sin^2 C}{\epsilon} + \pi \frac{\sin(P\epsilon + C) \sin((\pi - P)\epsilon - C)}{\sin \pi \epsilon}, \quad (\text{A9})$$

with  $C \equiv Pq + T$ . Inserting this result into eq. A7 we have the desired analytic expression for  $c_2$ .

- <sup>5</sup> P.Yeh, A. Yariv and A.Y. Cho, Appl. Phys. Lett. **32** (1978) 104-105.
- <sup>6</sup> W. Ng, P. Yeh, P.C. Chen and A. Yariv, Appl. Phys. Lett. **32** (1978) 370-371.
- <sup>7</sup> P. Yeh, A. Yariv and Chi-Shain Hong, J. Opt. Soc. Am. **67** (1977) 423-438.
- <sup>8</sup> A. Yariv and P. Yeh, "Optical Waves in Crystals", Wiley (New York), (1984) Ch. 6.
- <sup>9</sup> W.M. Robertson, J. Lightwave Technology, **17** (1999) 2013-7.
- <sup>10</sup> W.M. Robertson and M.S. May, Appl. Phys. Letters **74** (1999) 1800-2.
- <sup>11</sup> M. Shinn and W.M. Robertson, Sensors and Actuators **B105** (2005) 360-364.
- <sup>12</sup> F. Ramos-Mendieta and P. Halevi, J. Opt. Soc. Am. B **14** (1997) 370-81.
- <sup>13</sup> F. Villa, J.A. Gaspar-Armenta, F. Ramos-Mendieta, Opt. Commun. **216** (2003) 361-67.
- <sup>14</sup> F. Villa and J.A. Gaspar-Armenta, Opt. Commun. **223** (2003) 109-115.
- <sup>15</sup> J.A. Gaspar-Armenta and F. Villa, J. Opt. Soc. Am. B **21** (2004) 405-12.
- <sup>16</sup> G.V. Morozov, D.W.L. Sprung and J. Martorell, Phys. Rev. E **69** (2004) 016612 +11.
- <sup>17</sup> G.V. Morozov, D.W.L. Sprung and J. Martorell, Phys. Rev. E **70** (2004) 016606 +7.
- <sup>18</sup> D.W.L. Sprung, G.V. Morozov and J. Martorell, J. Phys. A: Math. Gen. **37** (2004) 1861-80.
- <sup>19</sup> I.S. Gradshteyn and I.M. Ryzhik, "Table of Integrals, Series and Products", Academic Press (New York) 1980.
- <sup>20</sup> Yong Xu, R.K.Lee and A. Yariv, Optics Lett. **25** (2000) 1756-8.
- <sup>21</sup> M. Ibanescu, S.G. Johnson, M. Soljačić, J.D. Joannopoulos, Y. Fink, O. Weisberg, T.D. Engeness, S. A. Jacobs and M. Skorobogatiy, Phys. Rev. E **67** (2003) 046608 +8.

---

<sup>1</sup> E. Moreno, L. Martin Moreno and F.J. García-Vidal, Phys. Rev. B **69** (2004) 121402R.

<sup>2</sup> E. Moreno, L. Martin Moreno and F.J. García-Vidal, Phot. and Nanostr. **2** (2004) 97-102.

<sup>3</sup> P. Kramper, M. Agio, C.M. Soukoulis, A. Bimer, F. Müller, R.B. Wehrspohn, U. Gösele and V. Sandoghdar, Phys. Rev. Lett. **92** (2004) 113903.

<sup>4</sup> A.I. Rahachou and I.V. Zozoulenko, "Waveguiding properties of surface states in photonic crystals", arxiv:physics/0510273



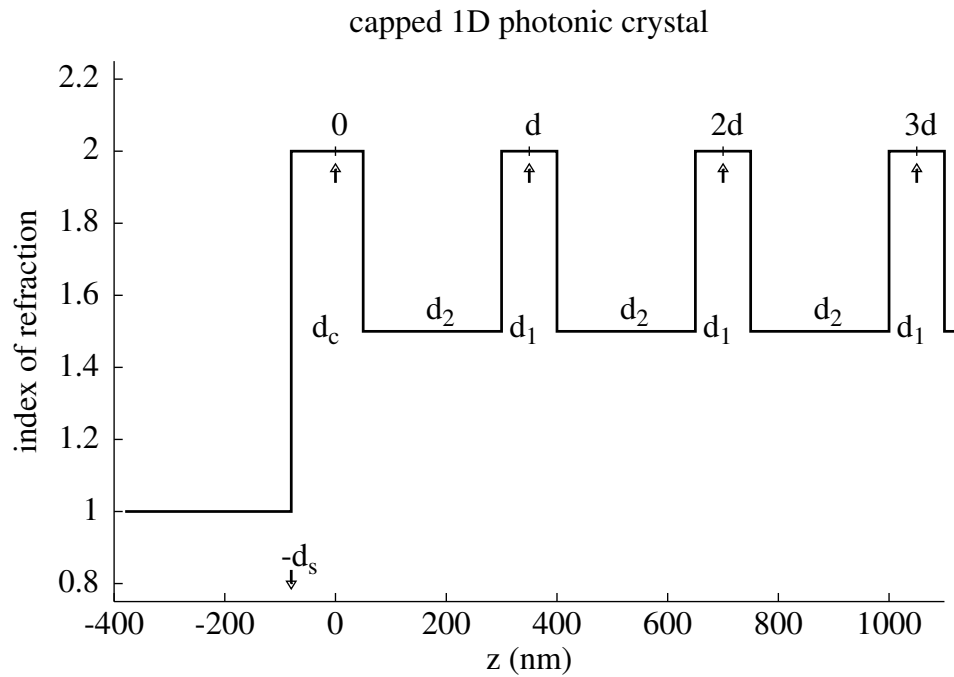


FIG. 1. Sketch of a typical 1D PC, for the case used in calculations ( $n_1 = 2.0$ ,  $d_1 = 100$  nm,  $n_2 = 1.5$ ,  $d_2 = 250$  nm.) A symmetric unit cell was chosen, and  $d_c = 80$  nm.

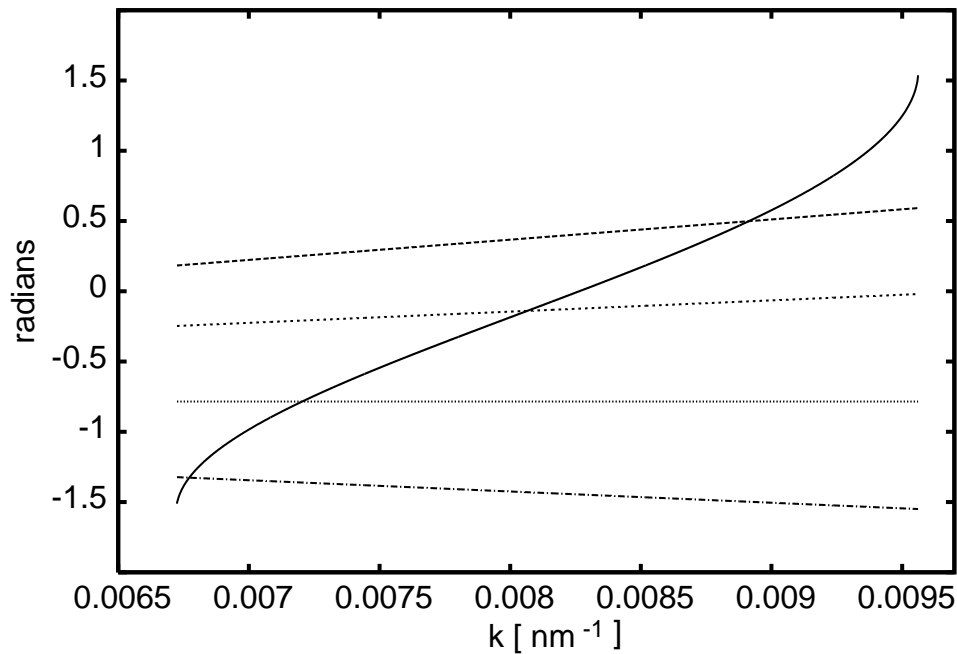


FIG. 2. Graphical solution of eq. 23 for  $n_0 = 1$ ,  $n_1 = 2$ ,  $d_1 = 100$  nm,  $n_2 = 1.5$ ,  $d_2 = 250$  nm. and  $\beta = 1.2$ . Continuous line:  $\theta_{\lambda-A}$ ; dashed straight lines: r.h.s. for several values, from top to bottom,  $d_c = 0.05, 0.25, 0.50$  and  $0.75d_1$ .

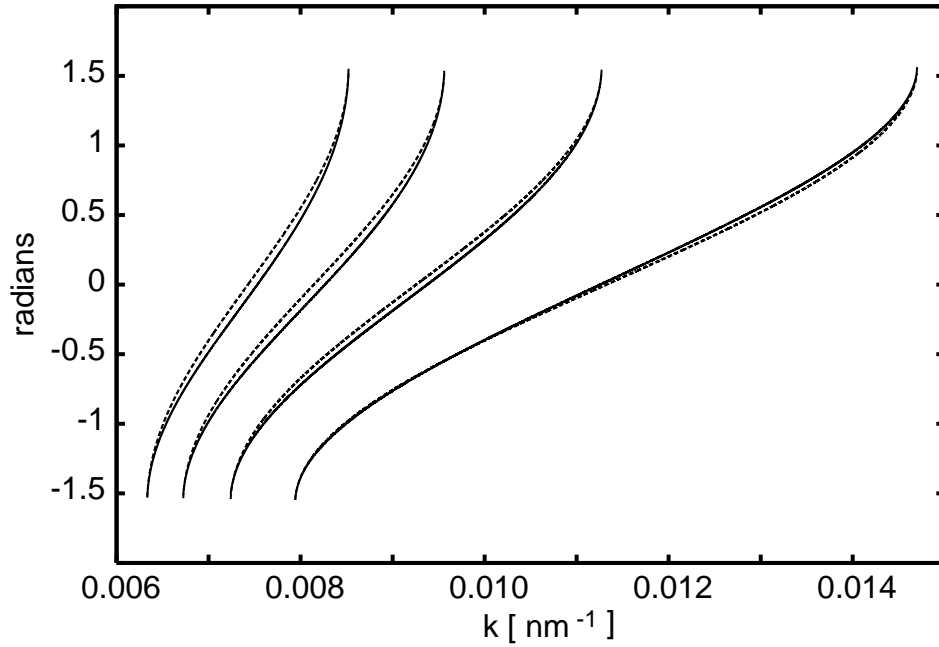


FIG. 3. Exact (continuous line) v.s. empirical approximation (dashed line) to the argument of  $\lambda - A$ . From left to right,  $\beta = 1.1, 1.2, 1.3$  and  $1.4$

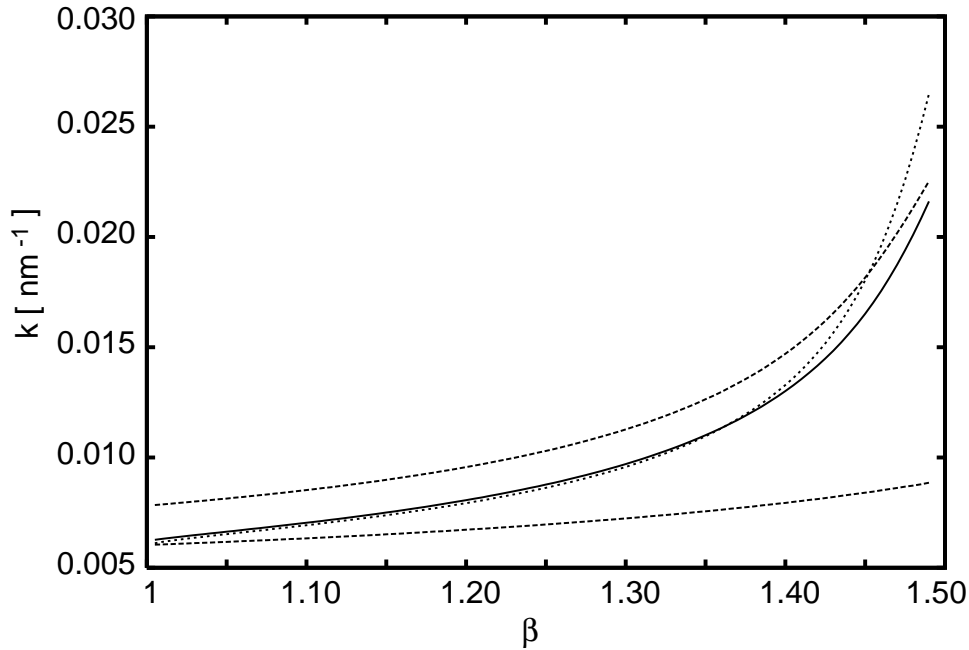


FIG. 4. Dispersion relation  $k = k(\beta)$  when  $d_c = 0.25d_1$ . Continuous line: exact solution of eq. 16. Dotted line: linear approximation, eq. 26, based on the empirical form of  $\arg(\lambda - A)$ . The dashed lines are the boundaries of the first bandgap.

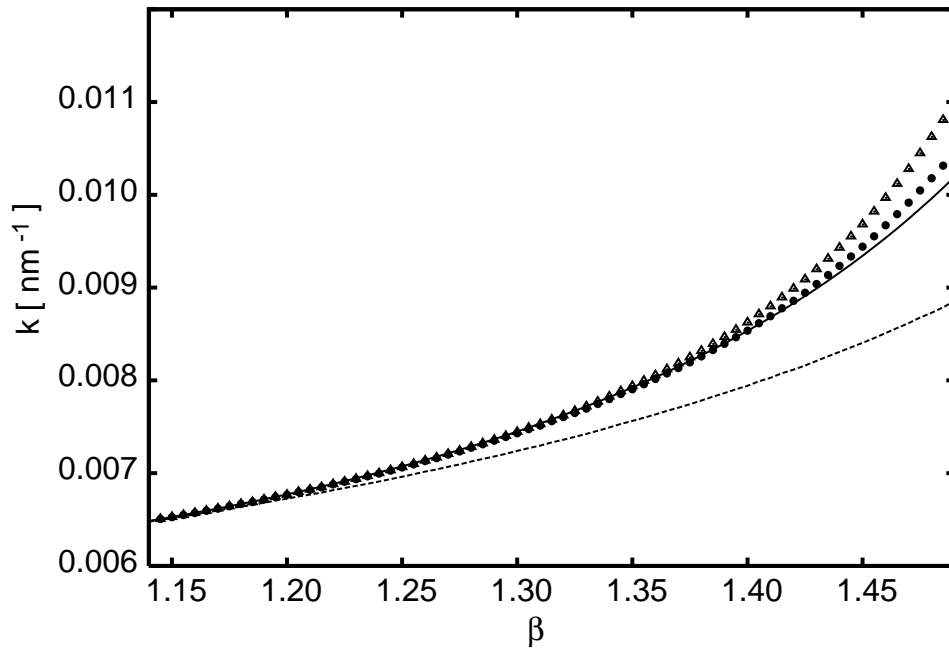


FIG. 5. Dispersion relation when  $d_c = 0.75d_1$ . Exact (continuous line) v.s. approximations based on the empirical form of  $\arg(\lambda - A)$ . Triangles: eq. 32; filled circles: eq. 31. The dashed line is the lower boundary of the first bandgap.

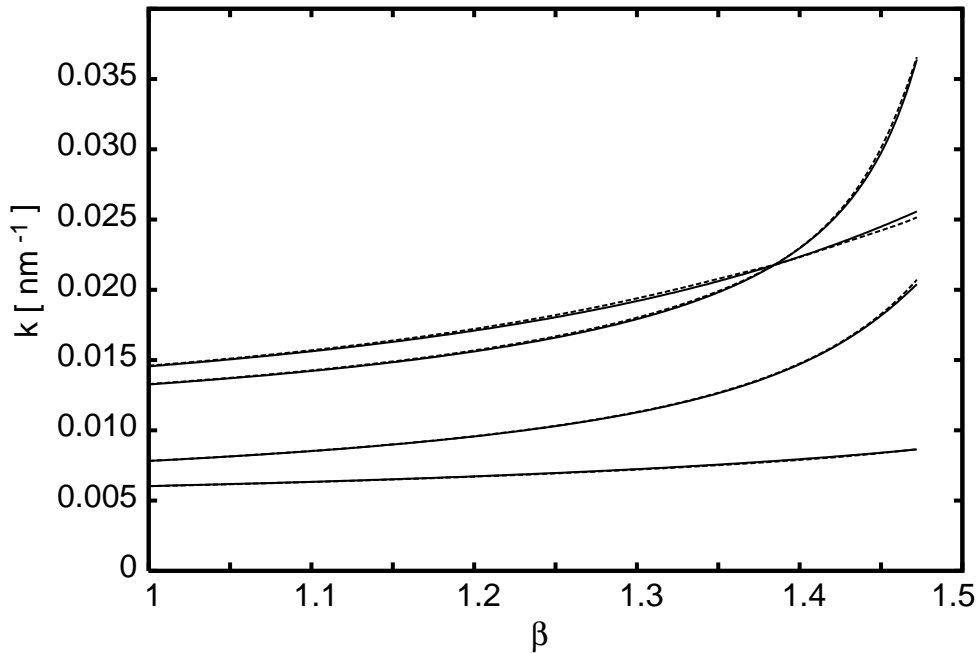


FIG. 6. First and second bandgap boundaries: Thin continuous lines: exact. Dashed lines: second semiclassical approximation described in text.

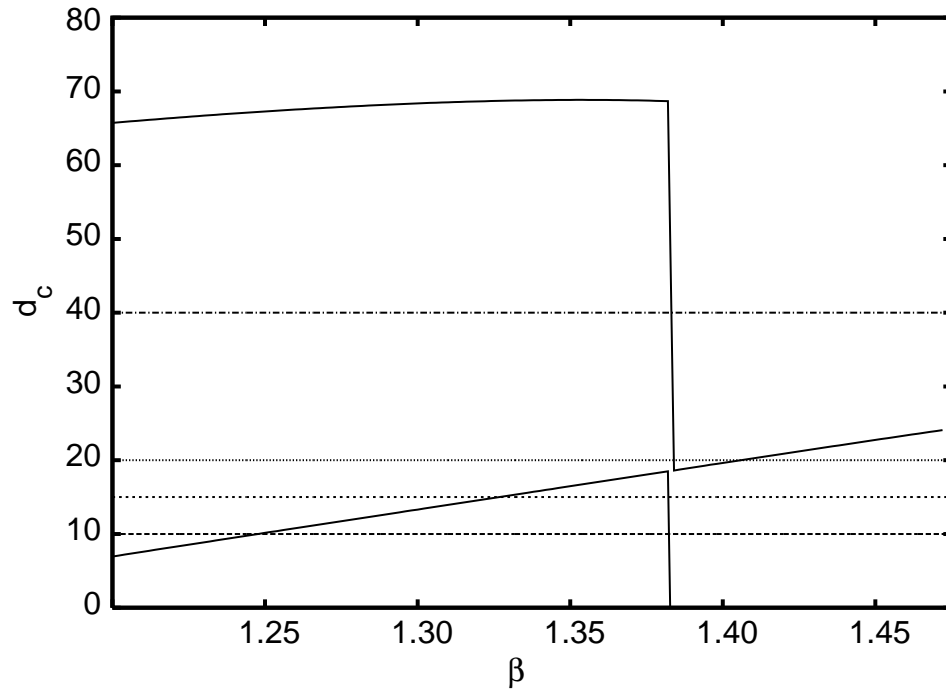


FIG. 7. Second bandgap: Continuous lines  $d_{c,min}$  and  $d_{c,max}$  as predicted from eq. 33. Dashed horizontal lines: from bottom to top  $d_c = 10, 15, 20$  and  $40$  nm.

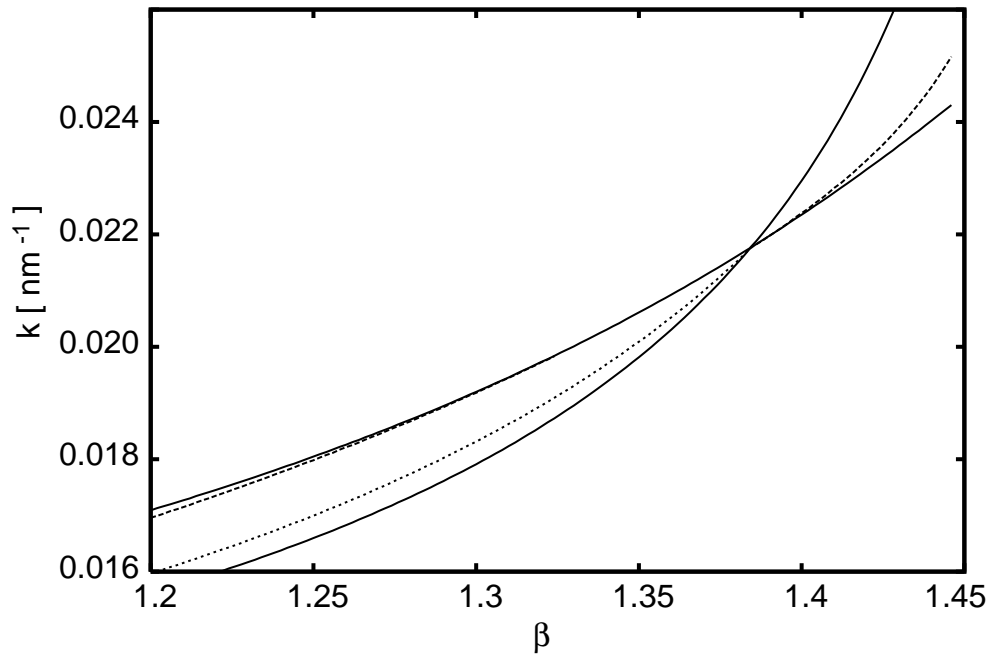


FIG. 8. Second bandgap: Continuous lines: zone boundaries. Dispersion relation for  $d_c = 0.15d_1$  (dashed line), and  $d_c = 0.40d_1$  (dotted).

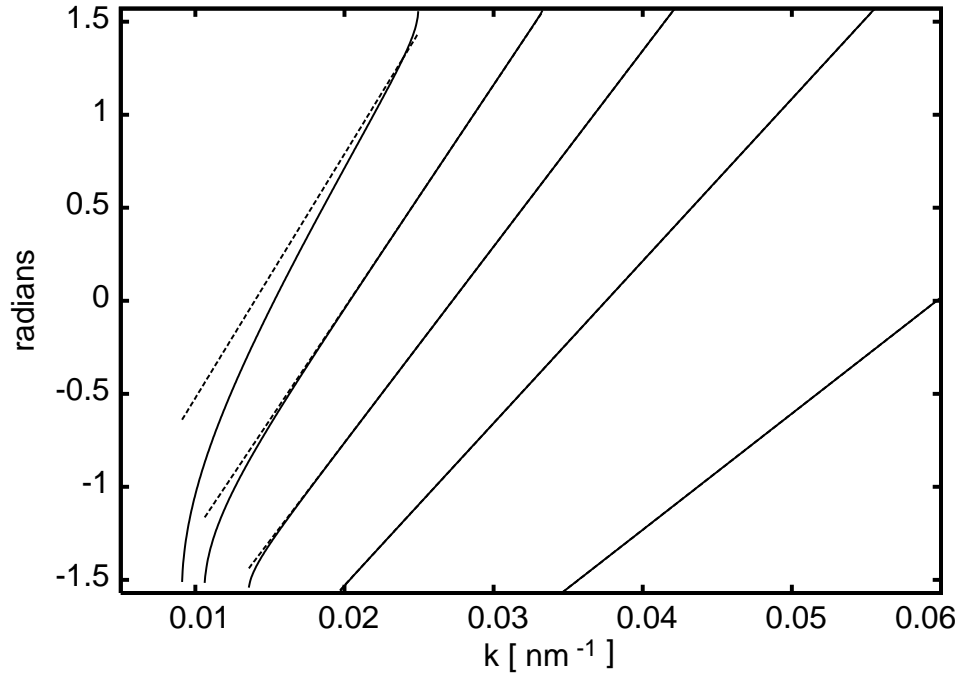


FIG. 9. Argument of  $\lambda - A$  in first bandgap. From left to right:  $\beta = 1.51, 1.6, 1.7, 1.8$  and  $1.9$ . Continuous lines: exact; dashed lines: linear approximation of eq. 42

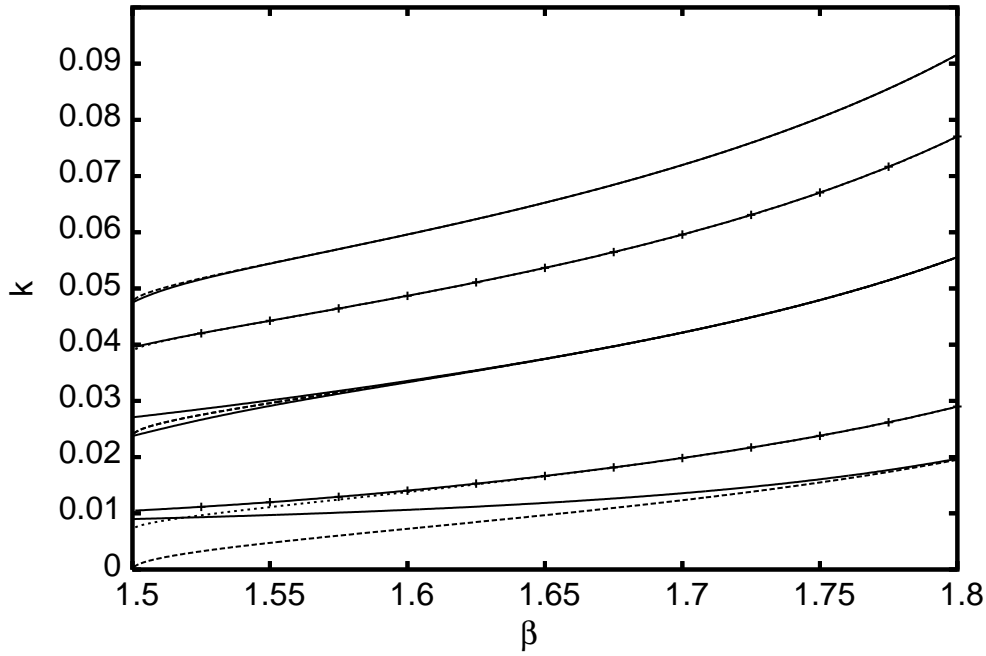


FIG. 10. First and second bandgaps when  $\beta > n_2$ . Continuous lines: exact boundaries. Dashed lines: approximation described in text. Surface waves: solid line with + symbols: exact; dotted lines: approximation given in the text.

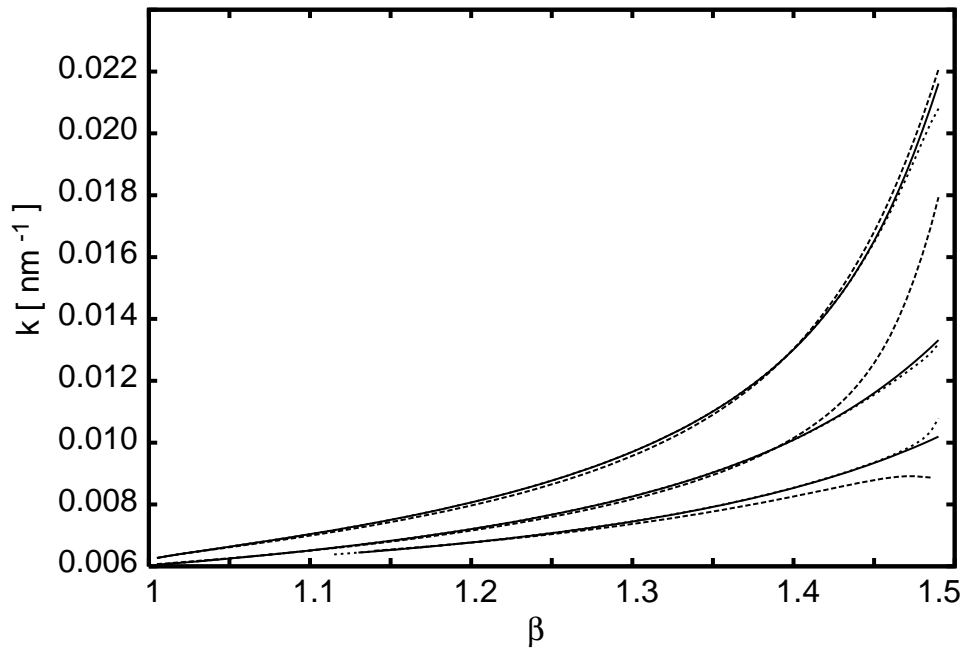


FIG. 11. First bandgap:  $k = k(\beta)$  curves for  $d_c = 25, 50$  and  $75$  nm. Continuous lines: exact. Long dashes: first approximation, short dashes: second approximation. The latter curves are so close to the exact ones that the difference can be seen only when  $\beta > 1.45$ .